Acta Polytechnica **61**(SI):14–32, 2021
DOI:10.14311/AP.2021.61.0014

available online at https://ojs.cvut.cz/ojs/index.php/ap

APPLICATION OF ADVANCED COMBUSTION MODELS IN INTERNAL COMBUSTION ENGINES BASED ON 3-D CFD LES APPROACH

Oldřich Vítek[a,*], Jan Macek[a], Vít Doleček[a], Zbyněk Syrovátka[a], Zoran Pavlovic[b], Peter Priesching[c], Ferry Tap[d], Dmitry Goryntsev[d]

[a] *Czech Technical University in Prague, Faculty of Mechanical Engineering, Department of Automotive, Combustion Engine and Railway Engineering, Technická 4, CZ-16607 Prague 6, Czech Republic*

[b] *AVL-AST d.o.o., Ulica kneza Koclja 22, 2000 Maribor, Slovenia*

[c] *AVL List GmbH, Alte Poststraße 152, 8020 Graz, Austria*

[d] *AVL Dacolt BV, Grote Looiersstraat 28, 6211 JJ Maastricht, Netherlands*

[*] corresponding author: oldrich.vitek@fs.cvut.cz

Abstract. This paper deals with the application of advanced simulation techniques for combustion modeling in the case of an internal combustion engine. The main focus is put on models with a high predictive ability hence 3-D CFD was selected while using LES (turbulence model) and detailed chemistry (both SI and CI ICE) or turbulent flame propagation (SI ICE). Both engine types are considered – spark ignited ICE and a compression ignited engine. Examples are shown and comparison with available experimental data is presented. The main conclusion is that such models are capable of high quality predictions while very little tuning is needed. This is desired as such models could be applied in the early phases of ICE development. On the other hand, such calculations are very demanding in terms of computational power.

Keywords: Internal Combustion Engine, 3-D CFD, LES, tabulated chemistry, ECFM, combustion, injector, spray.

1. Introduction

The main trend of ICE development in recent decades can be characterized by two main targets: to maximize engine efficiency and to minimize pollutant formation. In many cases, these two goals cannot be achieved simultaneously as improving the former leads to the worsening of the latter and vice versa. If these targets are to be achieved, detailed optimization of combustion process is necessary – this requires deep knowledge of all the important phenomena ranging from fuel injection to detailed chemistry including its interaction with turbulence. The latest trend is to combine dedicated experiments with advanced simulation methods. Regarding the latter, computational fluid dynamics (CFD) remains a useful tool.

A lot of progress has been made in the field of CFD in recent decades. That statement concerns all important topics related to ICE combustion: turbulence, spray, chemistry and turbulence-chemistry interaction (TCI). If applied correctly, the 3-D CFD could be especially predictive, hence allowing its use during the early ICE development phases to achieve the optimal design sooner.

1.1. Relation to work of prof. Kozel

The 3-D CFD simulations at the Department of Automotive, Combustion Engine and Railway Engineering of the Faculty of Mechanical Engineering at the Czech Technical University were started in late 1990's and the Ph.D. Theses aimed at CFD modeling from a numerical perspective were under prof. Kozel s supervision . This was a time when commercial CFD codes were of poor quality and it was necessary to use dedicated in-house codes which were developed only for special applications (e.g., internal combustion engines). The AMEM (arbitrary movable Eulerian model) algorithm applied in the case of an internal combustion engine was developed in [1]. Its extension from 2-D to 3-D was done in [2] – this included few 2-equations turbulence models and a turbulence driven combustion model based on the Level-Set approach. High pressure liquid fuel injection was developed in [3]. In all these cases, prof. Kozel was supervising the numerical methods to achieve a fast and stable solution of the turbulent unsteady compressible problem. Later on (the end of 1st decade of 21st century), the department stopped developing their own in-house codes – instead, well proven commercial 3-D CFD codes were applied (e.g., [4]). However, the lessons learned during the time of writing in-house codes proved to be extremely useful when applying the commercial CFD SW tools. This knowledge is considered to be very important and it is necessary to transform that for the young generation of researchers which prof. Kozel contributed to strongly.

Based on the above mentioned, the data shown in the paper can be considered to be the latest results of the department in the field of multi-dimensional

CFD thermodynamic modeling of internal combustion engines – the work which was started by prof. Kozel (among the others) some 25 years ago. And the results (shown in the section 6) were selected in such way to demonstrate the progress which was achieved during this time period. Hence, this paper is a tribute to the work of prof. Kozel in the field of internal combustion engine CFD modelling.

1.2. Paper goals

The presented work is focused on highly predictive combustion modelling 25 years ago, this was not possible as both the theoretical models (e.g., LES, ECFM, tabulated chemistry) and their numerical implementations were either not available or they were still in the early phases of their development. The main target is not to present completely new results. Instead the main goal is to show what is possible to achieve with the latest CFD tools and methods. To achieve that while giving some kind of overview of these methods, the majority of the results of the shown in this paper were already published. Hence, it combines the data/results from different research projects and also presents some new (unpublished) data as well.

This paper is focused on advanced ICE combustion modeling – different approaches were tested and compared with available experimental data while considering both SI ICE combustion mode and CI ICE one. Since there are many possibilities of combining turbulence models with dedicated combustion models, the review sub-section (which is usually positioned in the Introduction to give overview of state-of-the-art methods) is skipped. This paper is purely focused on very predictive models, hence the well-established LES approach was applied to model turbulence effects. The paper presents an overview of recent results (achieved at the Czech Technical University in Prague in close cooperation with AVL colleagues) in the field of highly-predictive combustion modeling.

Based on above mentioned, the following goals of the paper were set:

- To simulate the complete ICE cycle(s) using 3-D CFD approach while focusing on combustion phase using highly predictive models.
- To compare the results with available experimental data.
- To perform sensitivity studies of selected parameters.

2. Mathematical model

For the simulation of the gas flow, spray mixture formation and flame propagation processes in the internal combustion engine, the 3D-CFD code AVL FIRE [4] is adopted. The 3-D CFD SW solves the general conservation equations of mass, momentum and enthalpy plus additional transport equations for turbulence related quantities and for conservation of chemical species. Depending on the physical and chemical submodels employed, additional scalar quantities, such as mixture fraction, reaction progress variable, flame surface density, etc. are solved as well.

The adopted solution method is based on a fully conservative finite volume approach. All dependent variables, such as momentum, pressure, density, turbulence, kinetic energy, dissipation rate, and the scalar quantities are evaluated at the cell centres of the general, unstructured computational grids. A second-order midpoint rule is used for integral approximation and a second order linear approximation for any value at the cell-face. Convection is solved by adopting higher order differencing schemes. In order to offer full flexibility in terms of the structure and topology of the employed computational meshes, the solver allows for each computational cell to consist of an arbitrary number of cell faces. Connectivity and interpolation practices for gradients and cell-face values are set up to accommodate such 'polyhedral' calculation volumes. The rate of change (accumulation term) is discretized by using an Euler implicit scheme. The overall solution procedure is iterative and is based on the Semi-Implicit Method for Pressure-Linked Equations algorithm (SIMPLE) or Pressure-Implicit with Splitting of Operators (PISO, c.f. [5]), applicable to turbulent flows at all speeds. For solving the large sets of linear equation systems evolving from the discretization of the governing equations, an efficient preconditioned conjugate gradient method is employed. More details can be found in [6, 7] and documentation of AVL FIRE [4].

Dealing with numerical setup, the following settings were applied. PISO algorithm was selected as the overall solution procedure while 2^{nd} order schemes were used for convective term approximations. Time step was typically set to 0.1 degCA while shorter time step was applied during a combustion phase.

Regarding turbulence modelling, Large Eddy Simulation (LES) was adopted. It is based on the filtered instantaneous Navier-Stokes equations. Filtering operation actually represents scale separation in space, where large scales are directly resolved and the influence of small scales is taken into account by the sub-grid scale (SGS) model. Coherent structure version of LES approach [8–10] was selected. It is based on the eddy viscosity concept, but contrary to well-known Smagorinsky model [11], model parameter in CSM is not constant. It is locally calculated at each time-step and in each computational cell, based on the coherent structure function and the energy-decay suppression function, which are obtained from the resolved flow field. The coherent structure function is defined as the second invariant of the velocity gradient tensor normalized by the magnitude of a velocity gradient tensor, and its role is to provide appropriate damping near the walls, while the suppression function considers the suppression of the dissipation with the increase of an angular velocity. The main

advantages of the CSM model can be summarized as: it does not require a separate wall damping function, it can be also applied to laminar flow, there is no need for solving additional transport equations (e.g. for sub-grid turbulent kinetic energy), no averaged flow properties are required by the model, coherent functions have distinct upper and lower limits, which makes the CSM model very stable and robust.

The spray model adopted in the present study is based on the Lagrangian Discrete Droplet Method (DDM) [12]. In the DDM the continuous gaseous phase is described by the standard Eulerian conservation equations, whereas the transport of the dispersed phase is calculated by tracking the trajectories of representative droplet parcels. A parcel consists of a number of droplets, with all the droplets having identical physical properties and behaving equally when they move, break up, hit a wall or evaporate. The calculation of the parcel movement is done with a sub-cycling procedure between the gas phase time steps taking into account the forces exerted on the parcels by the gas phase as well as the related heat and mass transfer. The coupling between the liquid and the gaseous phases is achieved by source term exchange for mass, momentum, energy and turbulence. For the LES application, turbulent dispersion effects are assumed to be fully covered by the interaction of the droplets with the resolved LES flow field scales – hence, this term is deactivated when LES approach is applied.

Concerning combustion models, different approaches were applied depending on ICE type. For the case of SI engine (the Engine A – c.f. Table 1, Figure 1) the LES version of ECFM-3Z was activated due to positive experience with this model from the past – c.f. [6, 7]. Premixed turbulent SI-engine combustion is modeled in the present case by using the LES variant of the Extended Coherent Flamelet Model (ECFM) [13] which is based on solving a transport equation for the flame surface density (FSD), suitably linked with the gas-phase thermochemistry. It should be stressed that this model is turbulence driven, hence it cannot capture local chemical effects (e.g., flame quenching due to low temperature or turbulence-related effects) – this leads to a statement that all fuel is (usually) burnt when using this model (provided there is enough oxygen). Dealing with applied chemistry, the turbulence driven combustion models are usually linked with simplified chemistry approaches based on equilibrium. This was also the case for the presented CFD calculations. The only considered pollutant was NOx, however its formation was based on a standard approach [14], which is to solve certain equations of chemical kinetics.

Regarding the case of CI engine (the Engine B – c.f. Table 1, Figure 2), the FGM combustion model was applied. It allows to include state-of-the-art fuel chemistry reaction mechanisms in CFD simulations at very practical CPU costs. This is achieved by a chemistry pre-processing technique, which consists of pre-computing the detailed combustion chemistry, storing the relevant data in a look-up table(s) and interpolating from this table during the CFD simulations. The applied FGM combustion model, described in detail in papers [15, 16], has two main features:

- Chemistry tabulation based on auto-ignition trajectories of homogeneous fuel-air mixtures, computed with detailed chemical reaction mechanisms.
- Presumed-PDF turbulence-chemistry interaction (TCI) modelling, using a beta-PDF

The chemistry look-up tables are built up with the AVL TABKIN software package, which is a dedicated tool for the generation of CFD look-up tables for advanced combustion models. The look-up tables have five dimensions: pressure, fresh gas temperature (for heat losses), mixture fraction, mixture fraction variance (for turbulence-chemistry interaction) and progress variable. Table dimension limits and discretization are automatically set based on user input of key engine data. Different state-of-the-art mechanisms were tested – more details can be found in [17].

The CFD models are based on 2 existing engine geometries (c.f. Table 1, Figure 1 and Figure 2). 3-D CAD data of engine cylinder head, piston and liner (for both engine variants) were provided by engine manufacturers. All the necessary geometrical information was available, hence the meshing procedure could be started. The meshing itself was made by means of a hybrid meshing tool of AVL FIRE. Typical mesh cell size was set to 0.6 mm – this is based on experience from the previous work [2, 3] with LES approach to SI ICE modeling. The important parameters of applied meshes are summarized in Table 2.

3. Commputed cases

As mentioned above, 2 different engine cases were considered (Table 1, Figure 1 and Figure2). They are labeled as the Engine A and the Engine B. The Engine A is a unconventional SI ICE. It corresponds to gas SI ICE dominated by swirl, which is equipped with scavenged pre-chamber to be able to ignite very lean mixtures (hence, a turbulent flame jet ignition device is applied). Even though the combustion process in the Engine A is a turbulent deflagration flame, its shape is dominated by a turbulent flame jet shape, hence it is (in terms of its shape and time evolution) similar to combustion in CI (diesel) ICE. On the hand, the Engine B is a classical CI ICE and its combustion process consists of both typical CI ICE phases: premixed combustion one and mixing-controlled one.

The Engine A corresponds to experimental CNG SI ICE with scavenged pre-chamber. Moreover, the Engine A was heavily modified from its original version, which represents a light-duty CI ICE – hence, it is dominated by swirling in-cylinder motion while there is a significant bowl in the piston. Dealing with the Engine A, 3 different operating points were considered

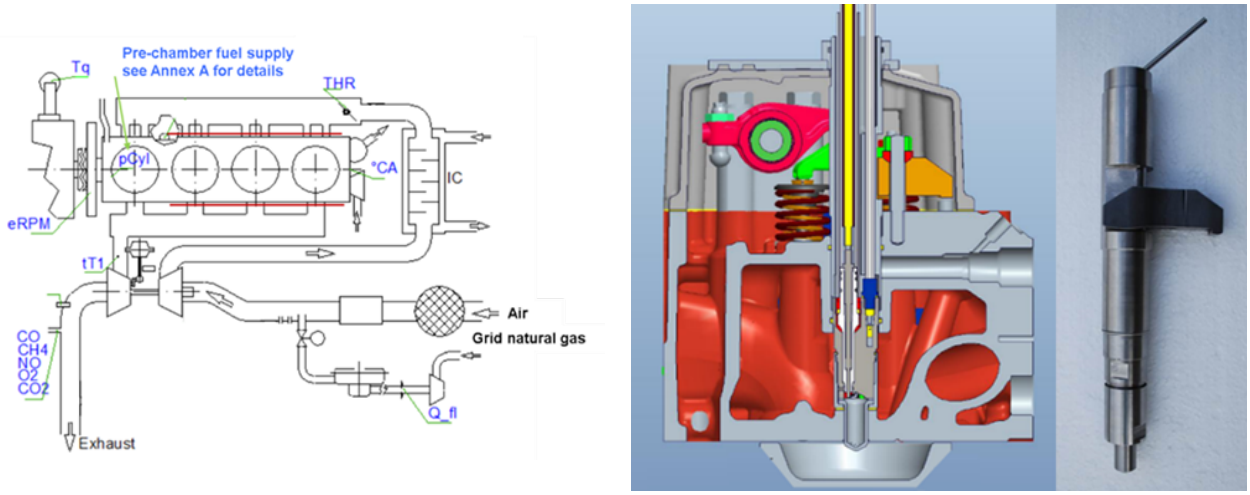

(A).

(B).

FIGURE 1. The Engine A – experimental single-cylinder research engine (SI version) equipped with scavenged pre-chamber.

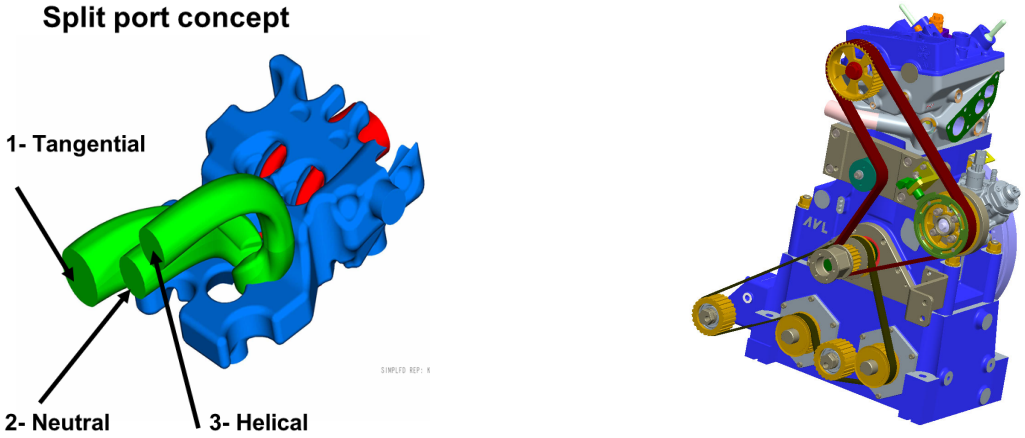

(A).

(B).

FIGURE 2. The Engine B – AVL single-cylinder research engine (CI version).

Engine Parameter	Unit	Engine A	Engine B
Bore-to-Stroke Ratio	[1]	0.850	0.944
Compression Ratio	[1]	12	15.9
Charging		Turbocharged	Supercharged
ICE Class		Spark Ignited	Compression Ignited
Fuel		Methane	Diesel
Fuel Injection		PFI + pre-chamber	Direct
Injection System		-	Common-rail
Injection Pressure	[MPa]	-	150

TABLE 1. Main engine parameters.

Engine Parameter	Unit	Engine A	Engine B
Typical Mesh Size	[mm]	0.6	0.6
Min. Amount of Mesh Cells	[1]	7.5M	3.0M
Max. Amount of Mesh Cells	[1]	13.0M	8.9M

TABLE 2. Main mesh parameters of full cycle ICE calculations.

Engine Parameter	Unit	Case A1	Case A2	Case A3
Engine Speed	[rpm]	1800	1800	1800
BMEP	[bar]	7.6	5.1	3.3
Total Inj. Fuel	[mg]	50.0	36.5	28.7
Air Excess	[1]	1.0	1.5	1.9
(external) EGR	[%]	0	0	0
Residual Gas Content	[%]	3.3	3.7	4.2

Table 3. Selected operating conditions of the Engine A.

Engine Parameter	Unit	Case B1	Case B2	Case B3	Case B4
Engine Speed	[rpm]	1500	1500	1800	1800
BMEP	[bar]	17.0	7.6	14.1	7.7
Total Inj. Fuel	[mg]	56.9	25.8	47.7	25.8
Air Excess	[1]	1.25	2.9	1.2	2.4
EGR	[%]	0	0	21	19
Residual Gas Content	[%]	6.6	7.1	26.7	22.5

Table 4. Selected operating conditions of the Engine B.

(c.f. Table 3) – these differ in air excess (un-throttled operation) ranging between 1.0 and 1.9 while engine speed was kept constant. Due to time demanding calculations, only 5 consecutive engine cycles were calculated. However, this should provide a good estimate of statistical moments of the 1st order (e.g., average values of scalar properties) – this observation is based on results from EU FP7 project LESSCCV, c.f. [6, 7]. More detailed information about the Engine A can be found in [18, 19]. The range of operating conditions related to data presented in the paper of the Engine A are summarized in Table 3. As the focus was also put on CCV effects, relatively low load cases were selected to avoid knock occurrence.

The Engine B (c.f. Table 1, Figure 2) represents the research single cylinder CI engine from AVL. There are many experimental data available for this engine. For the presented study, the single-pilot fuel injection pattern was adopted while combustion timing (location of 50 % burn point) was kept constant and while injection rail pressure was set to 150 MPa. The level of air excess (between 1.0 and 2.9 based on incoming fresh air) and EGR (between 0 and 22 %) were varied while engine speed was kept between 1500 and 2000 rpm. Hence, different engine load levels were achieved (BMEP between 7 and 17 bar). Due to very time consuming 3-D CFD calculations, 4 operating points were selected covering high/low BMEP at medium/low EGR level – these are summarized in Table 4. More detailed information about the Engine B can be found in [17, 20].

4. Model calibration

Concerning the Engine A model calibration, the following can be stated. For this particular case, there are only 2 combustion model parameters to be calibrated: initial flame surface density and turbulent flame stretch factor (the latter one is much more important). The values of these parameters were obtained by performing sensitivity studies of their influence for the Case A1 (c.f. Table 3). The calibrated model performance is shown in Figure 3, subfigures on the left side. Once a good match was achieved for the Case A1, all the model parameters were fixed for all subsequent calculations – there is one exception to that statement. As the standard ignition model was adopted (imposing flame kernel with predefined parameters: size, duration, flame surface density), it was necessary to find a correct phasing of this event. The ignition event was varied to match the 1st pressure peak in the pre-chamber – this was done for the 1st calculated cycle only while the same ignition phasing setting was kept for all subsequently calculated cycles of the same operating point. Hence, this adjustment was needed for every considered engine operating point.

Comparison between measured pressure traces and predicted ones is shown in Figure 3 – the left part represents almost stoichiometric conditions in a cylinder while the right one corresponds to very lean operation. Regarding the stoichiometric operation, there is a good correspondence, hence confirming satisfactory performance of the CFD model. This is also valid for CCV effects (cycles with the highest/lowest peak pressure are shown), hence the model was considered to be calibrated. On the other hand, the very lean operation (subfigures on the right side of Figure 3) is correct in only qualitatively – the reason is the fact that all the fuel is burned (in CFD calculation) while it is not the case for the target engine. More information can be found in [18, 19, 21–23].

Regarding CCV effects, there is a good correspondence between measurement and predicted data. However, the general observation is that the simulated pressure traces are over-predicted – when compared

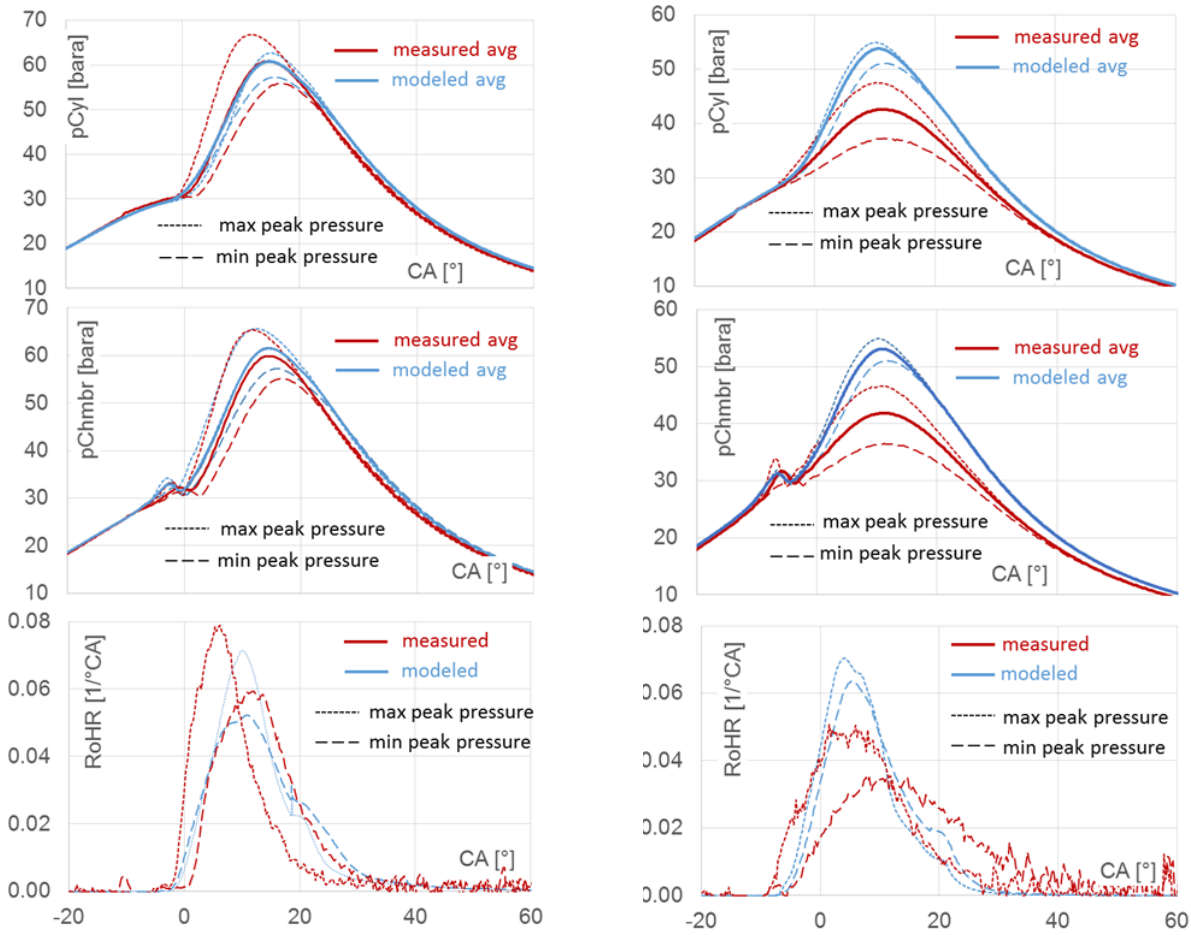

FIGURE 3. Comparison of measured and modeled pressure in the cylinder (pCyl - top) and in the pre-chamber (pChmbr - middle) and rate of heat release (RoHR - bottom) for the case of 1800 rpm and air excess of 1.0 (left; it is the Case A1 in Table 3) and 1800 rpm and air excess of 1.9 (right; it is the Case A3 in Table 3); blue color corresponds to CFD calculation, red color represents measured data, more details can be found in [21, 22].

with measurements, this is especially the case for operating points with high air excess. This is mainly related to the fact that the applied combustion model (LES ECFM 3-Z) is turbulence driven, hence it cannot predict possible local flame quenching (which is a chemical effect). That is the reason why all the fuel is always burnt in CFD simulations. This is not always the case for a real engine – up to 13 % of unburned methane was observed in raw exhaust gases when evaluating experimental data – the general trend is: the higher air excess, the more unburned fuel. The authors expect that low chemical efficiency (under high air excess operation) is related to local chemistry phenomena and their interaction with turbulence (that phenomenon is usually labelled as TCI). Only models based on chemical kinetics can capture these effects correctly – such models are currently under testing.

It should be mentioned that it was necessary to adjust a global heat transfer multiplier. This parameter is used to compensate for insufficient mesh resolution near the walls to predict correctly total rejected heat from the whole engine cycle. The data from calibrated 0-D/1-D model were used as reference. The final comment concerns the fact that this parameter has very little effect on ROHR.

Regarding the Engine B, the spray model had to be calibrated as it is well-known (c.f. [24]) that its time evolution is the most important single factor to influence combustion in direct injection CI ICEs. To calibrate a spray, experimental data are needed. In this case, the injection test bench EFS ITB 240 R-CV was applied – it is a cold pressure vessel device with optical access, which allows measuring rate-of-injection profile, injected mass, spraying cone angle and spray penetration length. Only liquid phase properties can be measured/evaluated as it is a cold device. More details can be found in [25]. Regarding the calibration procedure itself for the case of LES spray, the outcome was found satisfactory – Figure 4 shows the comparison of a calibrated model versus the experimental data. The LES spray model was calibrated for injection pressure of 160 MPa – its performance is equally good for lower injection pressure levels. More details can be found in [20].

Figure 5 shows the comparison of spray pattern time development between measurement and LES calculation. It should be stressed that the presented data

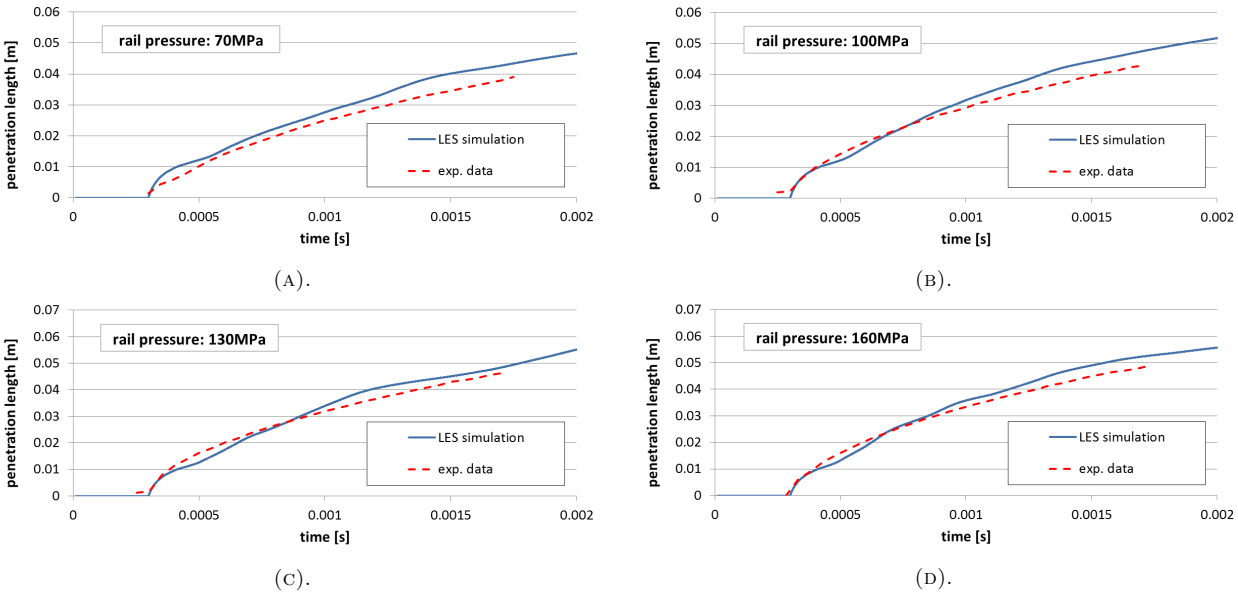

Figure 4. Comparison between measured data and calibrated LES spray model at different injection pressure levels while using data from cold pressure vessel – penetration length of liquid phase is plotted as function of time; LES spray model calibration was performed at injection pressure of 160 MPa, more details could be found in [17, 20].

are instantaneous ones and that the length scales are not exactly the same (when comparing experimental data and simulations). Hence, the figure is supposed to provide qualitative comparison only. Based on the figure, both the spray shape and spray cone angle are similar (when comparing simulations versus measurements) – this confirms good the performance of the calibrated LES spray model.

One of the main conclusions from the calibration procedure is that the mesh is the most critical factor – this is especially true for LES approach. The mesh must be capable of capturing very small structures that develop close to primary break-up zone. This requires a lot of mesh refinement along each spray nozzle axis – in this particular case, the smallest cells after refinement had a typical size of 0.075 mm when calibrating the spray in the constant volume vessel. However, such refinement is too fine for ICE applications as it would lead to a too large movable mesh (it might be even beyond the limit of what the solver could handle). Different meshes (for ICE calculations) were tested and it was found that the refinement of 0.15 mm is sufficient – this is related to the facts that in-cylinder temperatures are relatively high and turbulence level is higher, hence both evaporation and mixing is much stronger when compared with the case of a cold vessel. More details can be found in [20]. The above mentioned refinement was applied only during the injection period, hence the default mesh setting (c.f. Table 2) was considered in all other phases of 4-stroke engine cycle.

There are no direct parameters to be tuned when considering the combustion model itself – this is related to the fact that the model is based on chemical kinetics, hence all is driven by selected mechanism. After the calibration of the spray model was finished, the only other parameter to be adjusted (with relatively minor influence on important results) was a global heat transfer multiplier. It was necessary to tune its value due to the fact that correct heat transfer prediction is problematic in 3-D CFD (as it requires very fine mesh near the walls) – this is even more of an issue for LES cases as the 'wall function' approach cannot be applied. Details of heat transfer influence can be found in [20].

5. Numerical considerations

If using numerical methods for prediction of turbulent transport features, as diffusivity coefficient, temperature conductivity or kinematic viscosity, the impact of finite volume dimensions should be taken into account. The simple method that can show the limits of accuracy is described in the following text. It yields rather strict demands on mesh density but the experience from ICE simulations has proven the validity of estimation.

Let's assume the impact of the finite length of a FV on numerical diffusivity, defined by the concentration wave presence in the FV in consideration, i.e., the presence of the non-zero concentration of a specie transported by diffusion. Assume any concentration of the specie in consideration was present in a neighbor FV in a upwind direction during preceding time step. In the current time step a rather diluted specie occurs in the FV due to the homogenization of a FV contents after any time step. The concentration wave, although very diluted, spreads due to finite length and time steps as a false numerical diffusion with velocity, given by volume dimension and time step and the concentration increase during the time step. The

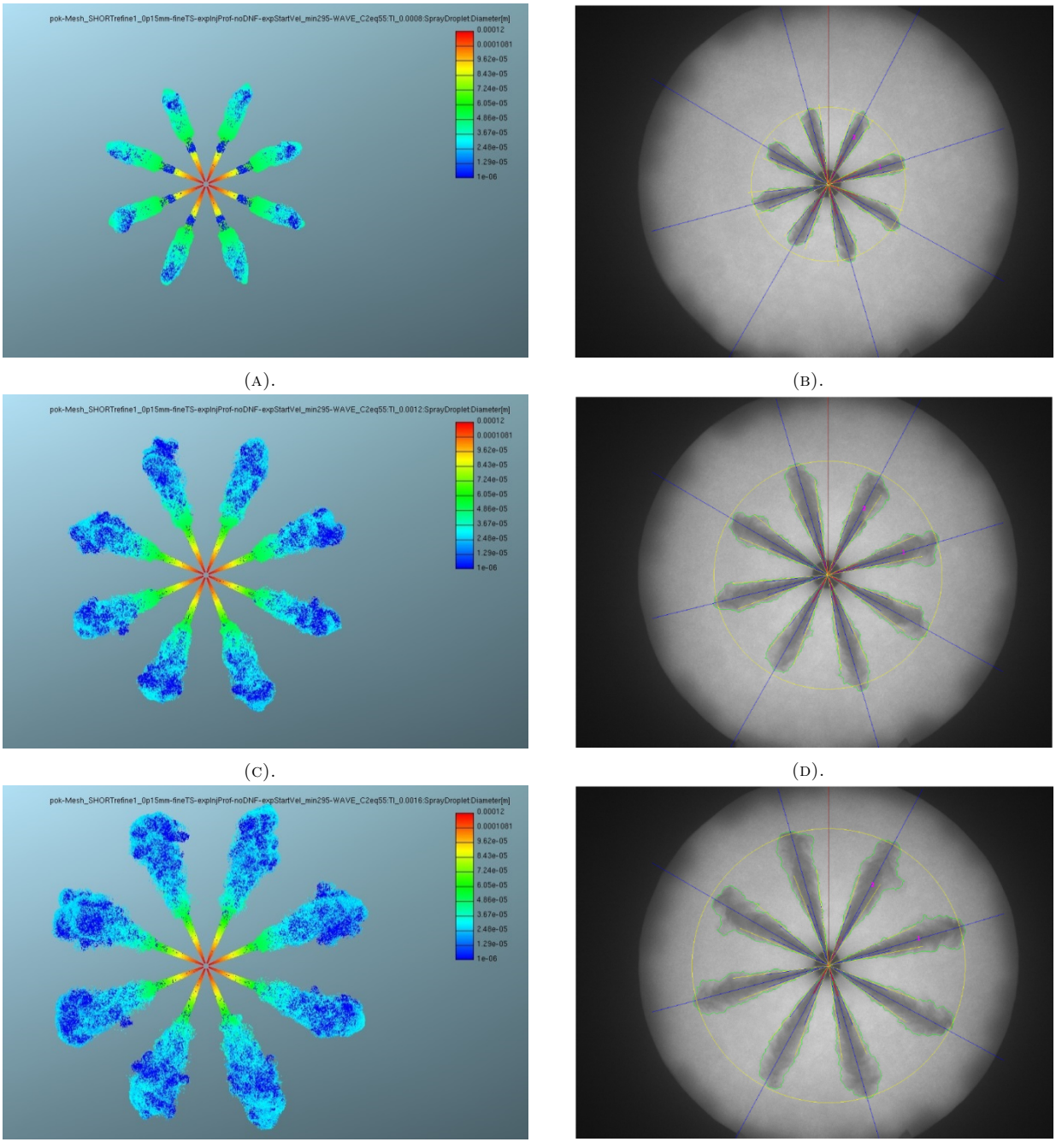

FIGURE 5. Calibrated LES spray model performance – spray pattern development in time domain at injection pressure of 160 MPa (time instances of 0.4, 0.8 and 1.2 miliseconds), left column corresponds to LES simulation (red color represent droplet size of 0.12 mm while dark blue one corresponds to 0.001 mm) while right column represents experimental data of a selected instantaneous injection shot (the scaling of length scale is approximately the same; penetration length comparison is shown in Figure 4, bottom right subfigure), more details could be found in [17, 20].

density of diffusion flux can be roughly estimated as

$$|\overrightarrow{j}| = |D\overrightarrow{\nabla} c| \approx D\frac{\Delta c}{\Delta x} \tag{1}$$

but simultaneously the fictitious velocity of propagation of concentration wave forehead through a finite volume FV is increased by fictitious numerical diffusion

$$\max|\Delta\overrightarrow{j}_{num}| = w_{overFV}\Delta c = \Delta D_{num}\frac{\Delta c}{\Delta x} = \\ = \frac{\Delta x}{\Delta t}\frac{\Delta c \Delta x}{\Delta x} = \frac{\Delta x^2}{\Delta t}\frac{\Delta c}{\Delta x} \tag{2}$$

and the increase of numerical diffusion coefficient is

$$\Delta D_{num} = \frac{\Delta x^2}{\Delta t} \tag{3}$$

The same procedure can be used for temperature wave, taking local thermal capacity of a FV into account

$$|\overrightarrow{q}| = \frac{\dot{Q}}{A} = |\lambda\overrightarrow{\nabla} T| = \lambda\frac{\Delta t}{\Delta x}; \\ \max(\Delta\dot{q}_{num}) = \frac{\Delta x^2}{\Delta t}\rho c_p\frac{\Delta T}{\Delta x} \tag{4}$$

Thermal conductivity may be estimated from it with the same result for temperature conductivity change as for diffusion coefficient. Numerical temperature conductivity increase is then equal to diffusion coefficient.

The yet unknown link between time and dimension steps yields CFL criterion ($CFL < 1$) while flow velocities inside a cylinder are usually limited by tens of meters per second

$$\Delta t < CFL\frac{\Delta x}{\max(w \pm a)} \tag{5}$$

which means

$$\frac{\Delta x^2}{\Delta t} > \frac{\Delta x \max(w \pm a)}{CFL} \tag{6}$$

Kinematic viscosity can be estimated from numerical Prandtl number, which should be equal to unity as it is roughly in all turbulence transport cases. Other possibility for the numerical distortion of kinematic viscosity is to use the mixing length model of turbulence, which yields similar results in orders of magnitude. Turbulent viscosity in internal combustion engines is according to experience approximately 1 000 times greater than a molecular one. It is valid even at the end of compression, where high density occurs without adequate growth of temperature, which reduces molecular kinematic viscosity. Numerical viscosity distortion should be a small part of turbulent one only.

The comparison of all transport coefficients to their molecular values shows the standard engine mesh size of $0.1 - 1$ mm is still too large/coarse, although even for automotive engines it needs $10^7 - 10^9$ mesh cells. Better meshes should limit the FV size less than 0.01 mm. It is still too fine for practical computing with meshes of 1 012 cells, if the full capacity of a supercomputer is not available. Sophisticated numerical methods of a higher order can shift this limit a little but not significantly, requiring not simple amendment of boundary conditions at solid walls.

The knowledge of the yet existing inaccuracy is very important if assessing the results of numerical simulations. They are very useful for mutual comparison with a similar mesh size but they have rare absolute validity.

6. Discussion results

This section contains selected results from different publications while some new results are shown as well. As the paper is supposed to provide an 'overview' of recent development/trends in the field of ICE combustion modeling, typical examples are presented without performing deep analysis. If the reader is interested in more details, there are references to the papers to provide more detailed information.

6.1. Results related to the Engine A

The most important results in terms of LES 3-D CFD for the case of gas (SI) ICE equipped with scavenged pre-chamber are presented in this section. It is based on data/results published in [19, 21–23]. The simulated data are compared with experimental/reference ones – the reference data correspond to calibrated 0-D/1-D model created in SW tool [26]. The reference data can give reasonable values of many integral data, which are not available from measurements.

It should be stressed that the Engine A is not a classical SI ICE. Its ignition system can be labelled as turbulent flame jet (more details can be found in [24]), which can be clearly seen in Figure 6. Even though it is SI engine dominated by deflagration flame propagation, the flame topology is different when compared with a classical spherical flame of SI ICE. Regarding CCV effects, the prediction matches experimental data well – c.f. Figure 3. The combustion is mainly dominated by a turbulent flame jet during early phase of in-cylinder combustion process – the jet is relatively strong, which leads to fast in-cylinder combustion. The turbulent flame jet is primarily driven by the pressure difference between pre-chamber main combustion chamber (cylinder), which is relatively similar when comparing different engine cycles – it seems that this phenomenon leads to the dampening of CCV effects taking place in pre-chamber. Based on all these facts, early flame kernel development phase (taking place in pre-chamber) seems to have a lower influence on CCV. Cyclic variation is mainly dominated by the turbulent flame jet development – this also includes its timing, which is slightly different among the cycles due to different pre-chamber combustion duration.

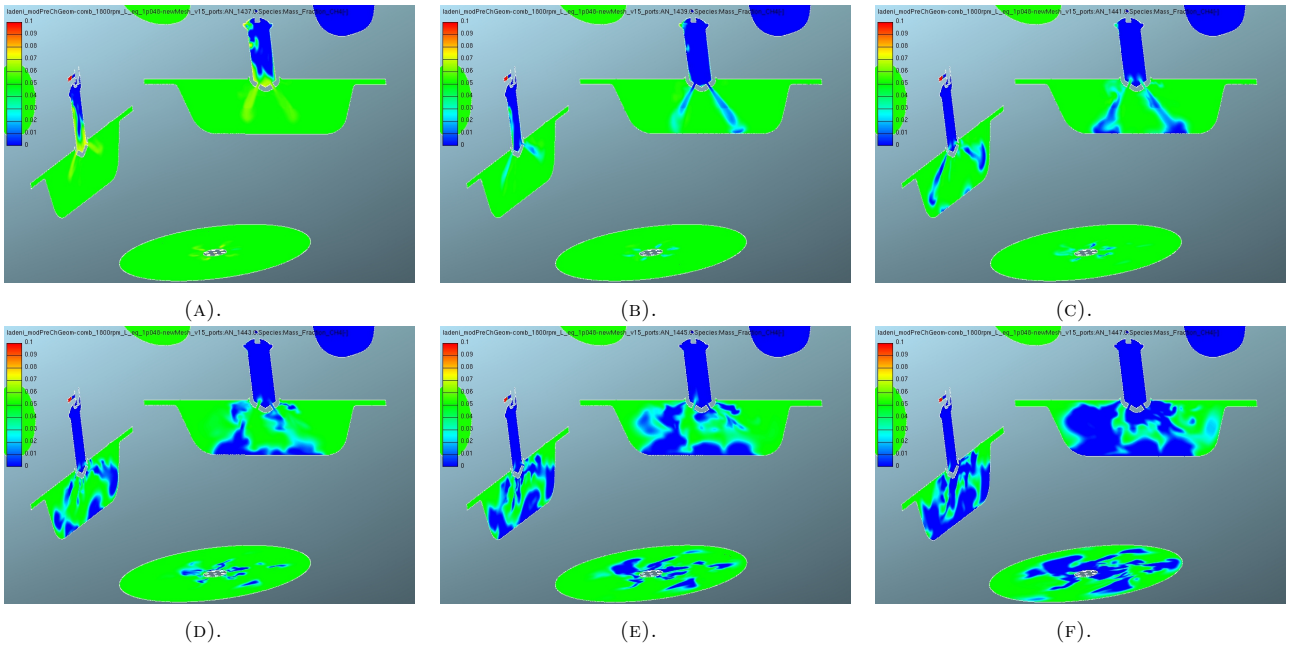

(A). (B). (C).

(D). (E). (F).

FIGURE 6. Flame development in time domain for 2nd calculated cycle – fuel mass fraction is plotted (blue color represents burnt zone – fuel mass fraction is zero) for the stoichiometric operation for the case of the Engine A (the Case A1 in Table 3); top row subfigures correspond to initial phase of combustion, every sub-figures represents an increase in time domain by 2 degCA (starting top left and moving to the right); more details could be found in [19, 21, 23].

Combustion progress in a cylinder of the Engine A is shown in Figure 3 (bottom sub-figures). Its shape seems to be similar for all calculated cycles while the main difference is combustion timing. Initial phase of in-cylinder combustion is primarily influenced by the turbulent flame jet, the timing of which corresponds to combustion progress in a pre-chamber – in other words: in-cylinder combustion starts only when the turbulent flame jet is initiated due to the flame front reaching connecting channels between a pre-chamber and a cylinder. The early phase of in-cylinder combustion seems to be nearly identical in terms of rate of heat release (c.f. Figure 3, bottom sub-figures) – up to approx. 30 % of burnt fuel, the slope of ROHR curve is almost the same for all calculated cycles. This suggests that early in-cylinder flame development, which is mainly dominated by the turbulent flame jet, is little dependent on instantaneous local thermodynamic status in both pre-chamber and cylinder. Hence, any local differences due to CCV effects (when comparing different cycles) are suppressed. Any visible CCV effects (in terms of ROHR) are developed only at later phases of the combustion process as turbulence needs some time to develop local differences, which lead to different rate of heat release.

Details of the combustion process in the Engine A are shown in Figure 6. Combustion in pre-chamber is similar to combustion in a classical SI engine, however CCV of mixture homogeneity is higher – this is mainly related to the swirling motion in pre-chamber coupled with small connecting channels. This phase is relatively slow. Once the flame reaches connecting channels (between pre-chamber and cylinder), there is a relatively high pressure drop (i.e., pre-chamber pressure is clearly higher than in-cylinder pressure), which leads to high flame jet velocities (reaching values up to 200 m/s). Hence, the flame jet reaches outer boundaries (e.g., piston top crown) very fast – this typically takes 2 degCA. After that, a complicated turbulent flame structure is being developed as a consequence of swirling in-cylinder motion and interaction among 12 turbulent flame jets. All that leads to fast combustion – in the case shown in Figure 6, it takes cca 10 degCA to burn all the mixture in the piston bowl region. The qualitatively same effects are observed even for cases of very lean mixture combustion. Hence, it confirms that turbulence is dominating the initial phase of combustion (i.e., up to the point of 30 % of burnt fuel).

It was decided to test the influence of pre-chamber size. The original pre-chamber design is labeled as 'small' – in this case, the pre-chamber volume is approximately 2 % of the in-cylinder compression volume. The pre-chamber was made larger (approx. by factor of 2) while the number and size of connecting channels remained unchanged – this pre-chamber design is labeled as 'big'. To verify scavenging strategies, some cases were run in 'passive' mode – no fuel scavenging is applied – this was tested for a large pre-chamber and it is labeled as 'big inscav'. These tests were performed both experimentally and virtually (simulations). It should be stressed that no model adjustments were made – its setting was exactly the same as for all previous calculations.

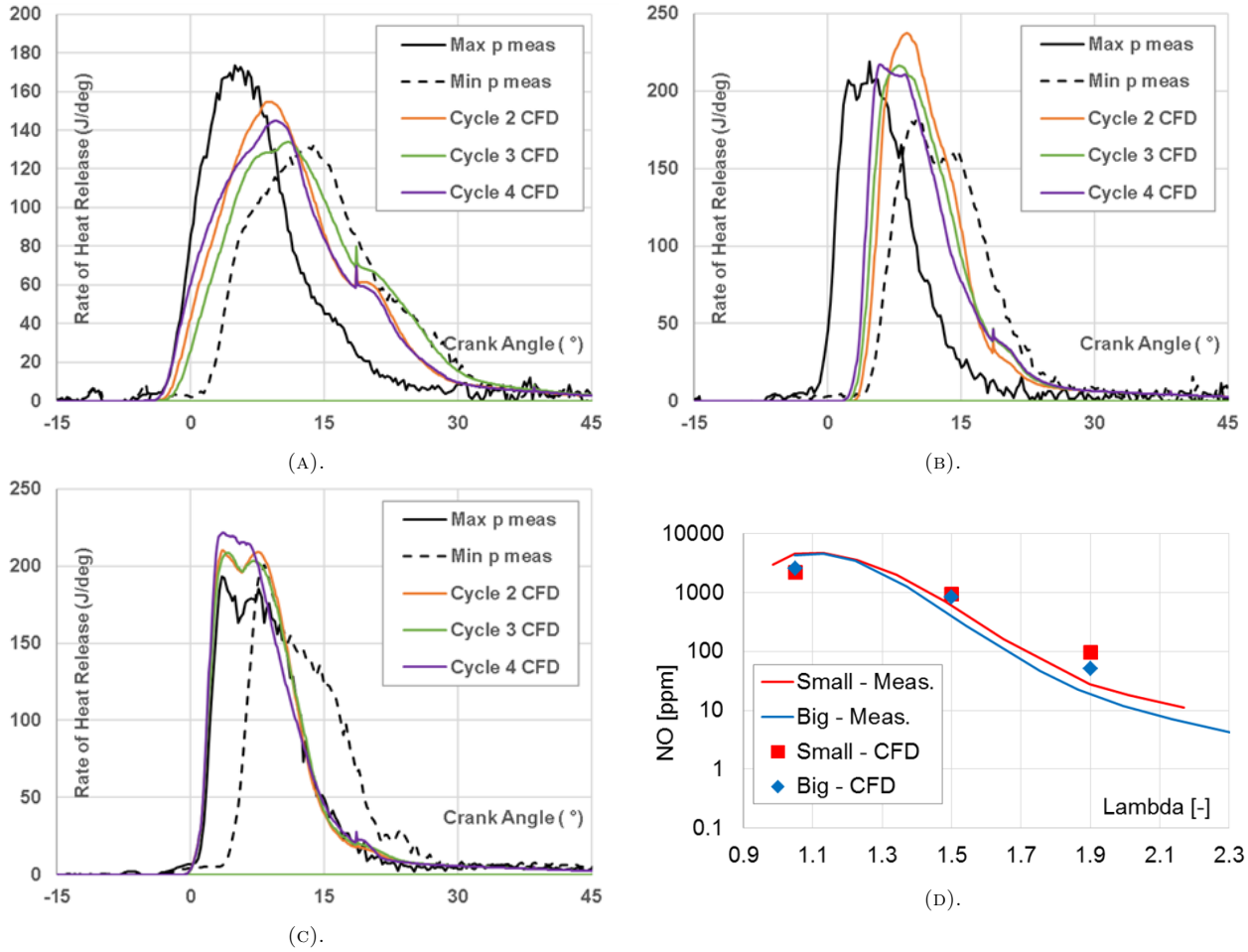

Figure 7. Comparison of individual cycle simulation data related to combustion (ROHR) at stoichiometric conditions (the Case A1 in Table 3) while comparing different pre-chamber design configurations (small/big) and scavenging strategies (scavenged/un-scavenged) – top left subfigure corresponds to standard/default pre-chamber (labeled as 'small'), top right represents enlarged design (label as 'big'), bottom left shows enlarged design without scavenging (labeled as 'big unscav'), bottom right subfigure presents NO formation; more details could be found in [22].

Figure 7 shows the comparison of in-cylinder ROHR traces among small pre-chamber, big one and big un-scavenged pre-chamber. Cycles with the highest and the lowest peak pressure (in the graphs labeled as 'Max p meas' and 'Min p meas') were selected out of 120 measured cycles. ROHR data from CFD calculations for the cycles 2, 3 and 4 are shown in the figure. All graphs correspond to the case of stoichiometric mixture quality and engine speed of 1800 rpm (the Case A1 in Table 3). The LES modeling approach is capable of predicting the variation of pressure traces for consecutive engine cycles – it captures the cycle-to-cycle variation (CCV), which is a typical feature of SI ICEs. Both the ROHR shape and its phasing are closely matched to experimental data. All CFD pressure traces lie within the limits of measured ones. Similar results were obtained for other operating conditions (the Case A2 and the Case A3 in Table 3). When comparing scavenging strategies, the following can be stated. The ROHR data shown in Figure 7 suggests that when big pre-chamber is applied, combustion becomes faster regardless of its operation mode (scavenged or un-scavenged) – ROHR of a small pre-chamber is clearly slower when compared with both cases of the big one. This is confirmed by experimental data as well, although the variant of scavenged big pre-chamber might be slightly overestimated by the considered CFD model.

Based on the above-mentioned and analysis in [19, 21–23], it was confirmed that combustion models based on turbulent flame front propagation cannot capture TCI effects (e.g., local flame quenching). Hence, it was decided to a test combustion model based on detailed chemistry. Based on experience from [17, 20, 27], it was decided to use the tabulated chemistry (labeled as 'TABKIN') – such a model is based on FGM approach. Hence, the same combustion model was applied as it is the case for the Engine B (more details can be found above – section 2, part dedicated to FGM model). The applied mechanism was GRI 3.0 (c.f. [28]). However, it should be stressed that there are some technical difficulties in applying SW tool [4] at the moment – the AVL colleagues are aware of that and substantial code development (related to these

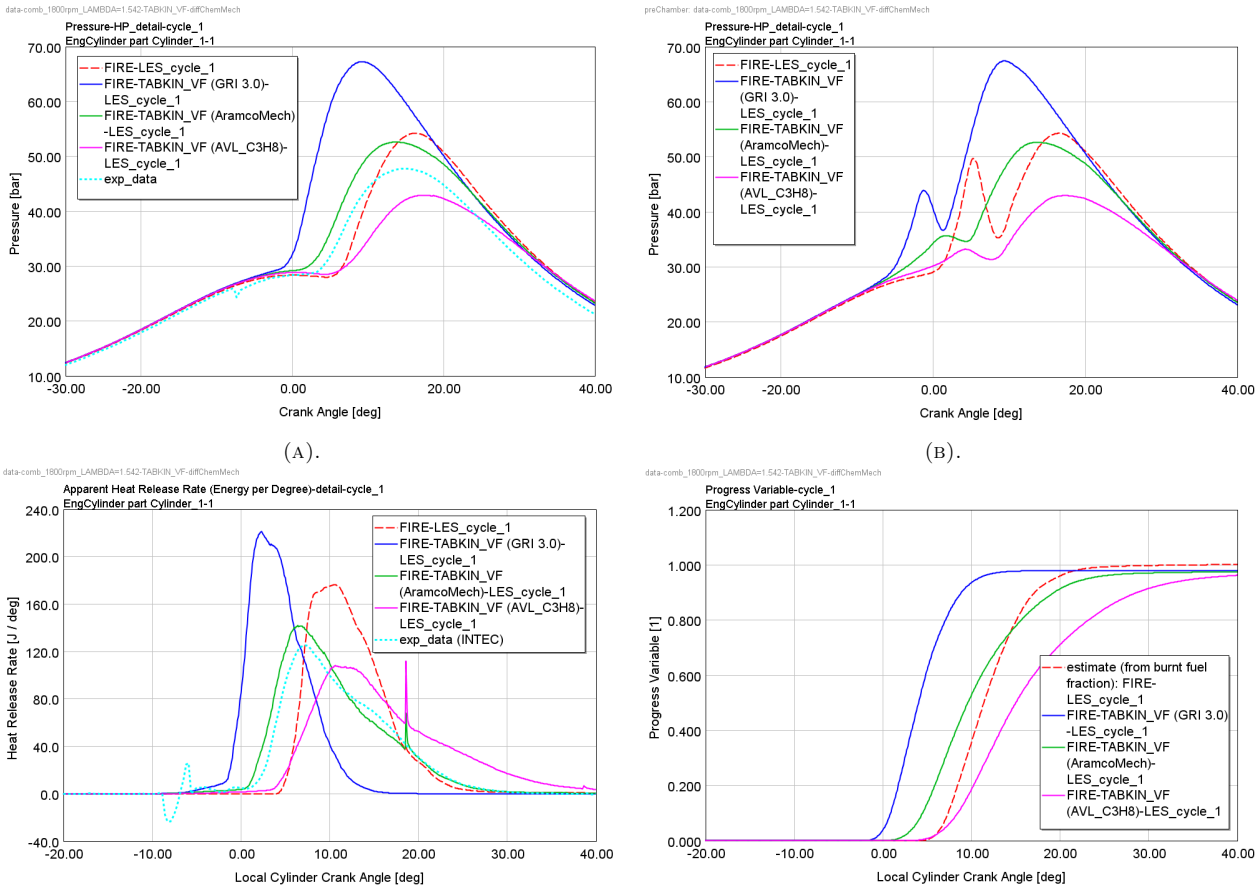

FIGURE 8. Comparison of 1st cycle simulation data related to medium-lean conditions (the Case A2 in Table 3) while comparing different combustion models (no label corresponds to ECFM, label 'TABKIN' represents FGM combustion model while considering different chemical mechanisms) – top left subfigure corresponds to in-cylinder pressure, top right represents pre-chamber pressure, bottom left shows in-cylinder ROHR, bottom right subfigure presents in-cylinder HR.

issues) is in progress. Hence, the presented data represent the first attempt and further progress is expected in the near future. Moreover, the SI combustion mode is more difficult to predict (when compared with CI one) due its strong interaction with local turbulence and its very small scales (comparable to Kolmogorov length scale) – more details can be found in [24].

Figure 8 shows selected data from the initial application of FGM combustion model for the case of SI ICE with scavenged pre-chamber – it is a medium-lean condition case (the Case A2 in Table 3) while using enlarged pre-chamber design. Although the data look reasonable, there are visible differences when compared to ECFM model, which matches experimental data reasonably well. It should be stressed that the 1st cycle is shown in Figure 8 while it was mentioned above that it is not recommended to present the 1st cycle (due to the fact that it is relatively strongly influenced by imposed initial conditions – hence, a relatively large difference to the measured average cycle is visible in the figure). However, due to the above mentioned limitations of the applied CFD tool [4], it is not possible to run multiple cycle calculations at the moment. From a general point of view, it seems that the FGM model predicts a faster ROHR – this was expected as applied mechanism (GRI 3.0) is relatively simple while it is well-known that simple mechanisms usually over-predict chemical activity. On the other hand, the AVL mechanism based on C3H8 hydrocarbon shows relatively slow combustion. The best performance seems to be obtained by means of ARAMCO mechanism, which is the most complex one (out of those tested). Bottom right sub-figure of Figure 8 shows that less chemical energy was released for the case of the FGM model (when compared with ECFM model) – this is another issue to be solved by means of the code modifications.

An example (one of many, which are typically carried out during a research project) of a sensitivity study is shown in Figure 9 (corresponds to in-cylinder data) and Figure 10 (represents pre-chamber data) – the data correspond to the influence of different geometrical configurations regarding the connection channels between pre-chamber and main combustion chamber (i.e., ICE cylinder). The label of each variant provides information about the amount of the chan-

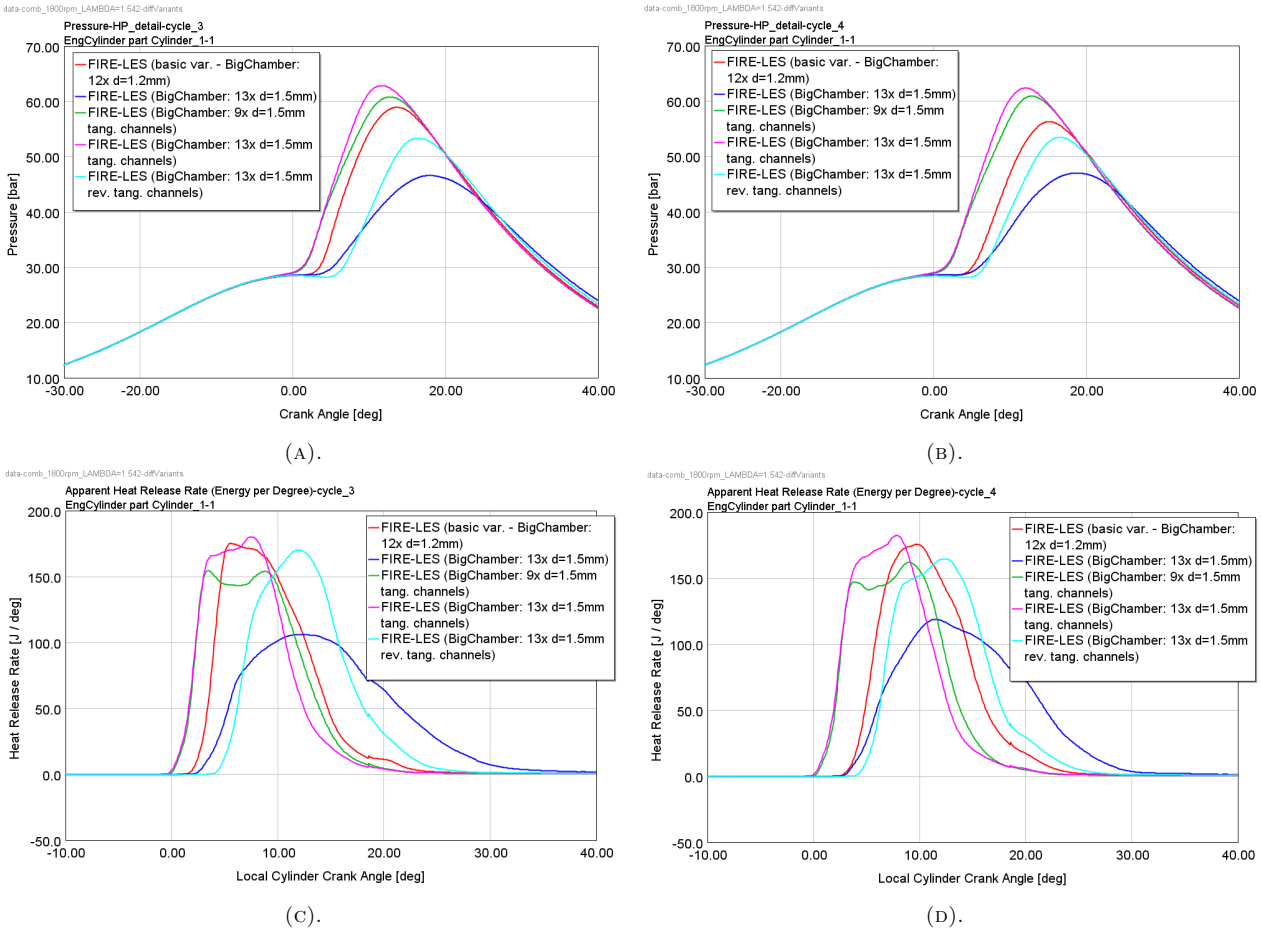

Figure 9. Comparison of simulation data (LES ECFM combustion model) related to medium-lean conditions (the Case A2 in Table 3) while comparing different pre-chamber designs (left column data: 3rd simulated cycle; right column data – 4th cycle) – top left/right subfigure corresponds to in-cylinder pressure, bottom left/right shows in-cylinder ROHR.

nels, their diameter and possibly about their space orientation (default value is a radial direction). As it is the LES calculation using ECFM combustion model, multiple cycles were calculated – the presented data correspond to the 3rd and 4th cycle, hence it allows to estimate CCV phenomenon as well. Dealing with the presented results, the following can be stated. If the diameter of the hole is increased (compare the red curve, which corresponds to a base variant with connection channel diameter of 1.2 mm, with dark-blue one), it leads to a significant decrease of combustion speed (ROHR) which is mainly related to slower exit velocities (from pre-chamber to main combustion chamber) of the flame jet. If larger holes are used while decreasing their amount to keep the total connection surface area at approximately a constant level (green curve), ROHR remains similar as well. If larger holes are applied while changing their space direction (default connection channel direction is a radial one) in such a way that it creates a strong swirling motion inside a pre-chamber (magenta curve), ROHR is increased significantly when compared with the case of radial direction (dark-blue curve). However, if the channels are orientated in the opposite direction (light-blue curve), the ROHR is delayed (due to longer flame development in the pre-chamber) and it is clearly slower than the original variant (magenta curve). The reason behind that is the relative orientation of those tangential channels with respect to in-cylinder swirl (created during the intake stroke by means of suitable positioning of intake ports) is important – if it is 'aligned' (magenta curve) during the late compression stroke, when the pre-chamber is filled by lean mixture from the cylinder, strong swirling motion is created in the pre-chamber, which increases turbulence level and mixing – all that leads to the faster combustion process in the pre-chamber, hence faster exit velocities of the turbulent flame jet, hence faster ROHR in the cylinder as well. On the other hand, if this is not the case (light-blue curve), the positive effect is much weaker, however it is still faster than the case with radial channels (dark-blue curve).

The final comment concerns the effect of CCV – the analysis of multiple cycle data suggests that the variants with tangential channels feature lower variations of ROHR. This should be the outcome of the swirling motion inside the pre-chamber, which stabilizes conditions there, increases mixing and turbulence. On the

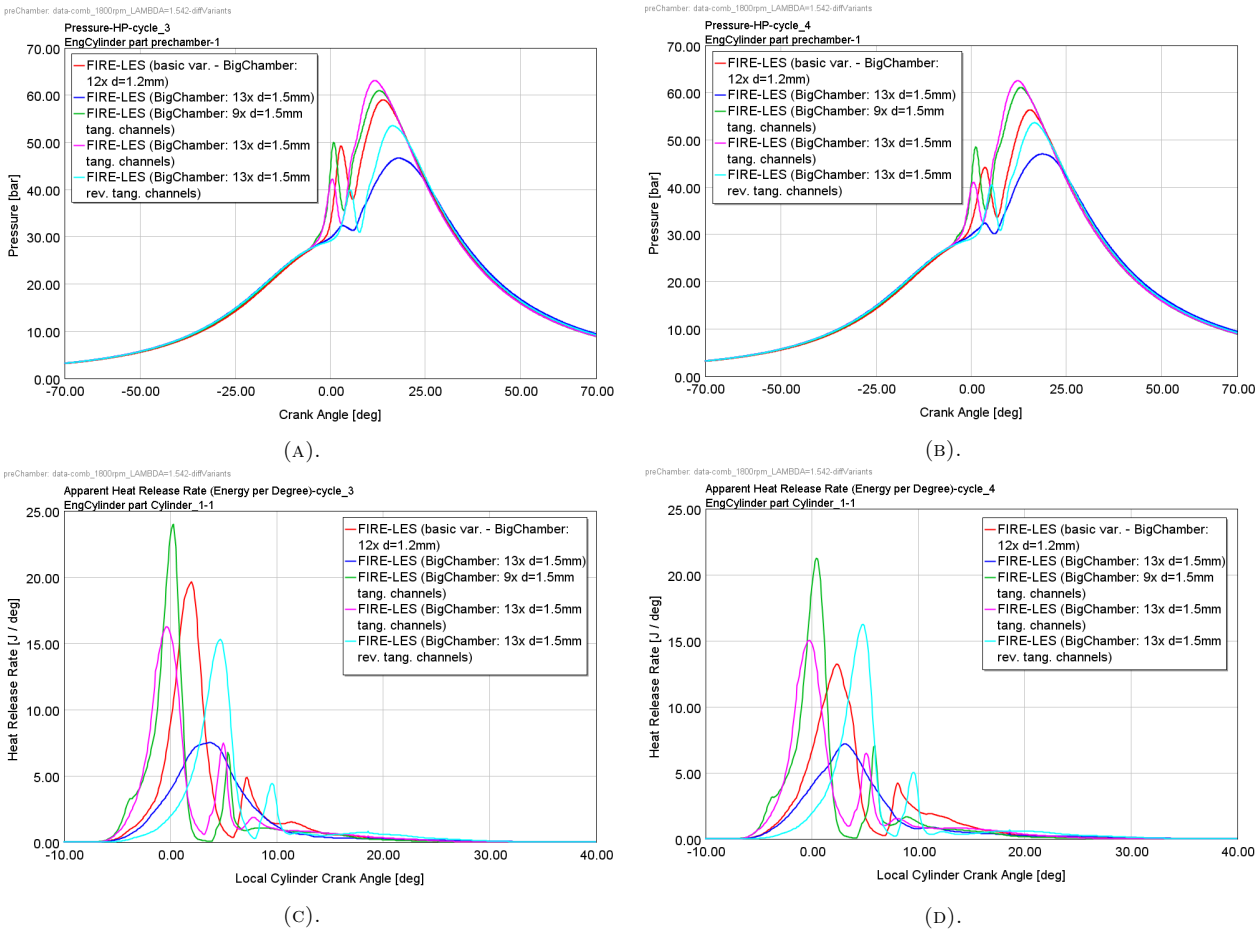

FIGURE 10. Comparison of simulation data related to medium-lean conditions (the Case A2 in Table 3) while comparing different pre-chamber designs (left column data: 3rd simulated cycle; right column data – 4th cycle) – top left/right subfigure corresponds to pre-chamber pressure, bottom left/right shows pre-chamber ROHR.

other hand, the swirling motion pushes (non-swirling) burnt/exhaust gases, which stayed in the pre-chamber from the previous cycle, towards the center line of the pre-chamber, hence closer to a spark plug. This might lead to possible issues with reliable spark event in the pre-chamber – this phenomenon was observed experimentally for some similar designs. As the combustion model (LES ECFM) is turbulence driven, its sensitivity to local chemical composition is low, hence its ability to predict such behavior is relatively low.

6.2. RESULTS RELATED TO THE ENGINE B

The most important results concerning diesel (CI) ICE while using LES 3-D CFD are presented in this section. It is based on data/results published in [17, 20, 27]. The simulated data are compared with experimental/reference ones – the reference data are based on a calibrated 0-D/1-D model built in SW tool [26]. The reference data provide reasonable values of important integral data, which may not available from measurements.

The base variant is labelled as 'GGPR_reduced_NC7' (it is based on a reduced version of NC7 mechanism: 34 species, 64 reactions; it is represented by red-dotted curves in the figures) and it represents a simple approach typically applied in industry – the chemical equations are directly solved during CFD calculation at every time step. Despite activating a 'clustering' method to speed up the numerical solution, it is much slower than all the cases which are based on the approach of tabulated chemistry. This leads to the fact that such an approach is not feasible when dealing with advanced mechanisms (which are typically based on hundreds of species and thousands of reactions). Three different state-of-the-art mechanisms from LLNL were tested – more details about these mechanisms can be found in [17]. This paper is not focused on comparing standard approach (based on a direct solution of chemical kinetics; labelled as GGPR) with tabulated chemistry one (labelled as FGM/TABKIN). That would be a relatively difficult task as these approaches are significantly different when concerning certain important details of their respective applications in CFD codes.

The comparison between simulation and experimental data in terms of apparent ROHR is shown in Figure 11 (the 'kink' shown in Figure 11 near 10 degCA represents a rezone, which 'confuses' the algorithm to evaluate ROHR from pressure data – hence, it is

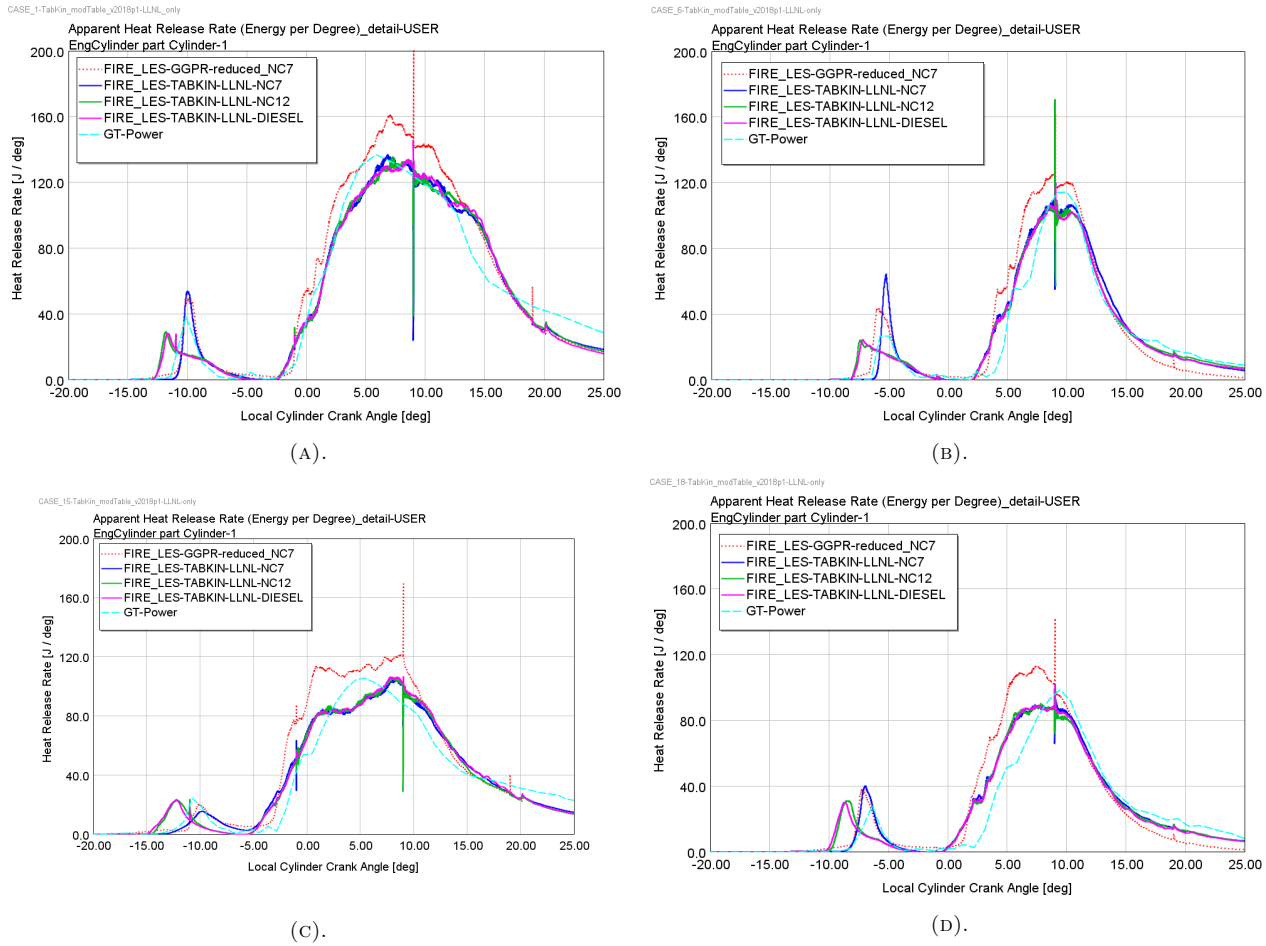

Figure 11. Comparison of apparent ROHR for the Case B1 (top left), the Case B2 (top right), the Case B3 (bottom left) and the Case B4 (bottom right) while considering different detailed mechanisms from LLNL (more details can be found in [17]); red color represents a reference calculation using GGPR approach, dashed lines correspond to experimental data (either measurement or calibrated system model based on 0-D/1-D).

an artefact which should be disregarded). A general statement is that ROHR is predicted reasonably well. There is a visible difference in the early combustion phase which corresponds to pilot injection/combustion. Mechanisms based on NC7 (hydrocarbon consisting of 7 carbon atoms) seem to predict both ignition delay and burning of pilot-injected fuel better than those based on NC12. Tested mechanisms based on NC12 are more complex (when compared with NC7-based ones), however they predict higher cold flame activity – this results in shorter ignition delay(s). This statement is confirmed by all considered load cases. On the other hand, ROHR is very similar during the main injection event – the only exception is the GGPR case, which is clearly faster during the early part of the main combustion phase. However, this was no surprise as it is well-known that small/simple mechanisms tend to predict clearly faster ROHR when compared with complex ones. From a general point of view, all tested mechanisms are visibly faster (in term of ROHR) at the beginning of the main combustion phase – this is one of the reasons behind the in-cylinder pressure over-prediction (pressure traces are not shown due to paper size limitations). This is even more visible for cases when high EGR was applied (i.e., the Case B3 and the Case B4). However, the final comment is that predicted ROHR is relatively similar to a measured one (represented by data labelled as 'GT-Power' which is a TPA-calibrated 0-D/1-D model of the target engine).

The data shown in Figure 11 also confirm the fact that the prediction quality of EGR influence is relatively poor. The applied EGR (c.f. Table 4) is only on a medium level (approx. 20 %) of what is typical for passenger car CI ICEs. Despite that, the ROHR is visibly different (when compared with the one without EGR) – it is clearly slower with lower ROHR peak. Slower combustion is predicted by all mechanisms, however there is bigger difference between experimental and simulated data (when compared with cases when no EGR is applied) – this concerns both the early part of main combustion shape and ROHR shape in general. This was also the case when the authors tested other chemical mechanisms from open sources.

As described above, predicted ROHR is reasonable but not perfect – it is certainly good enough from an engineer's point of view. It should be stressed again that very little tuning was necessary and it can be

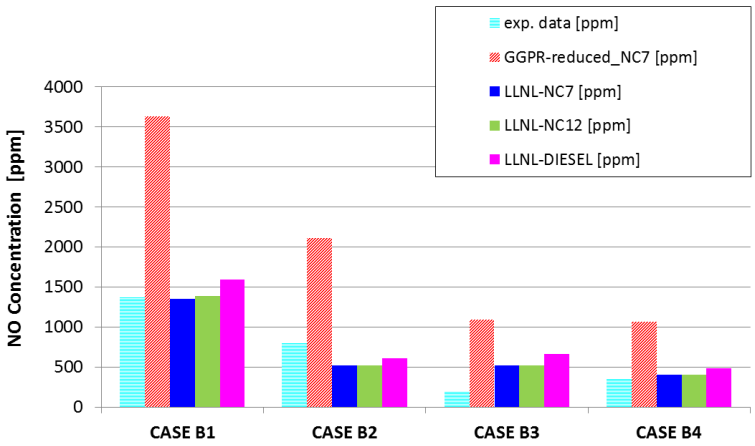

FIGURE 12. Comparison of NO emissions for all considered cases (B1, ..., B4); red color represents a reference calculation using GGPR approach, dashed light-blue bars correspond to experimental data; more details can be found in [17].

stated that the main combustion parameters (ROHR shape, ROHR phasing) are predicted relatively well, which confirms the fact that such CFD models have a very high predictive ability. Based on the authors' experience, such models are suitable for typical ICE optimization tasks (e.g., injection strategy, injector properties, combustion chamber shape). It is strongly recommended to apply the predicted ROHR (from 3-D CFD) in a calibrated 0-D/1-D model to obtain a more precise estimate of the target engine performance (e.g., ISFC/BSFC, IMEP/BMEP, heat transfer).

Figure 12 shows results related to NOx – the measured data are compared with the predicted ones. It is clear that the models based on tabulated chemistry are following the experimental data much more precisely. This is mainly caused by better ROHR prediction, which leads to a more realistic local temperature - and better chemical description of NO formation (which was transferred from GRI 3.0 mechanism) – this suggests that the classical Zelodovich mechanism [14] is too simplified for detailed 3-D CFD calculations. There is little difference among tested complex mechanisms, however the most complex one (labelled as 'LLNL-DIESEL') seems to be a bit better than the others.

To verify the predicative ability of the model (LES + chemical kinetics), it was compared to the results of when the Engine B was operated at different engine speed (2000 rpm), different injection pressure (70 MPa) and different compression ratio (14.0) while the engine load was similar (BMEP of 12.1 bar), no EGR was applied – c.f. Table 1 and Table 4 for reference setting and operating conditions. Example of such a comparison is shown in Figure 13. The quality of the predicted data is similar to the cases presented above despite significantly different operating conditions. It should be stressed that the model was not adjusted – the only change needed was the mesh due to different compression ratio.

Regarding the CPU performance demands, the following can be stated. Single table generation (using AVL TABKIN SW tool) takes approximately 48 hours while using 200 CPU cores and the corresponding 3-D CFD calculation takes approximately 36 hours on 128 CPU cores. If the same calculation were performed while using industry-standard approach (direct solution of chemical equations while using 'reduced' mechanism and applying 'clustering' approach to speed up the numerical solution), it would take approx.. 160 hours (7 days) on 128 CPU cores. Moreover, the chemical table can be re-used for many simulation/engineering tasks (e.g., when optimizing injection strategy). Hence, the tabulated chemistry approach is currently a very attractive option – it improves the simulation results quality (due to application of state-of-the-art mechanisms) while it can significantly decrease the calculation runtime. On the other hand, it is fair to say that there are still some technical issues to be solved, hence more development is needed before wide industry application is possible.

7. CONCLUSION

This paper is focused on the modelling of combustion in ICE. The main emphasis is put on highly predictive models so that they could be applied also in the early phases of ICE development. That is why the LES approach was adopted for turbulence modeling. Both ICE types were considered – unconventional SI ICE equipped with scavenged pre-chamber (labeled as the Engine A in the paper) and classical CI ICE (labeled as the Engine B). Regarding the applied combustion models, the following can be stated. As the interaction between chemistry and turbulence is important, the models based on solving equations of detailed chemistry (i.e., chemical kinetics) are needed. This seems to work reasonably well for the classical CI CIE, however it is trickier for SI ICE – the reasons behind that statement are related to the different nature of

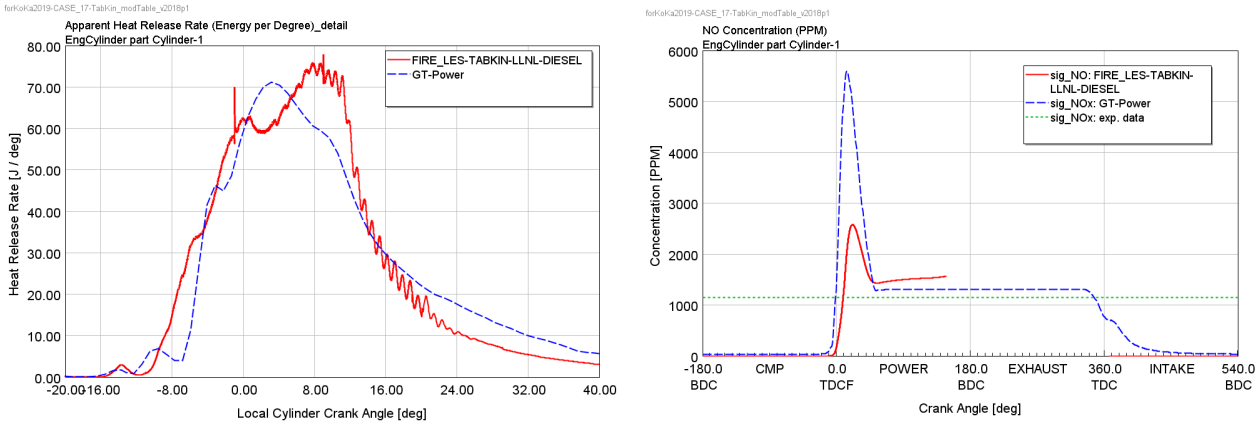

(A). (B).

Figure 13. Comparison of apparent ROHR (left) and in-cylinder average NO concentration (right) for the case of injection pressure 70 MPa, compression ratio of 14 at engine speed of 2000 rpm; dashed lines correspond to experimental data (either measurement or calibrated system model based on 0-D/1-D).

the flame (when comparing SI ICE with CI ICE). However, combustion models based on resolving local turbulent burning speed (e.g., ECFM) seem to work fine even for the case of unconventional SI ICE. The final comment concerns the fact that 'proper' combustion modeling with high predictive ability requires high quality modeling of turbulence, spray, mixing and heat transfer – this implicitly includes mesh effects (resolution, topology, local refinement, etc.) as well.

Dealing with SI ICE, the following can be stated. The standard approach of SI ICE combustion modeling is to resolve turbulent flame front propagation inside an ICE combustion chamber. This seems to work well when LES approach is applied. The statement was confirmed even for the case of ICE equipped with scavenged pre-chamber. Detailed analysis of 3-D CFD results shows that the combustion process of ICE equipped with pre-chamber is very complex. The flame structure is very different when compared with a classical spherical flame front shape of typical SI ICEs – its space distribution (shape) and topology is more similar to a classical direct injection CI ICE, although it is still a process based on deflagration flame front propagation. On the other hand, it was also confirmed that such models cannot predict TCI effects which lead to local flame quenching – this is experimentally observed when ICE is operated under very lean conditions. Hence, models based on chemical kinetics are needed.

Initial testing of the combustion model based on a solution of detailed chemistry was performed – it is the same approach (FGM combined with tabulated chemistry) as the one applied for CI ICE (the Engine B) presented in this paper. Although the initial results look promising, certain technical issues were discovered, hence substantial code development was scheduled. A relatively simple mechanism was applied (GRI 3.0) which resulted in the over-prediction of ROHR – this was expected based on experience with simple mechanisms. Further testing/development is planned for near future.

Regarding CI ICE, it is possible to state the following. If combustion models are based on detailed chemistry together with LES, such simulations are both time demanding and challenging. There are methods to speed up such calculations (e.g., clustering) – despite that, the direct solution of equations of chemical kinetics are very expensive from a simulation time point of view. Approaches based on tabulated chemistry offer a possibility to significantly speed up a numerical solution related to chemical processes – it should be mentioned that additional effort is needed to generate these tables. Once the tables are available, the CFD calculations are much faster (when compared with the classical way of directly solving equations of detailed chemistry) – this statement is valid regardless of the chemical mechanism complexity. Additional benefit is the fact that if the simulations need to be re-run (e.g., application of different sub-models, optimization tasks, sensitivity studies), the same chemical tables can be applied again. Hence, the tabulated chemistry approach allows to apply complex chemistry in every-day applications – this also includes the commercial sector.

Concerning the performance of tabulated chemistry, the following was found out. First, the simulation results correspond well with the data predicted by the classical (direct) solution of chemical equations. This statement concerns both ROHR and ignition delay. Second, when complex chemistry is applied, it brings significant improvement in terms of prediction quality when comparing it with simplified mechanisms (i.e., 'reduced' ones). Third, simulated NO data follows the trends from measurement while it allows for clear improvement when directly compared with the classical Zeldovich mechanism, which is a widely applied standard in ICE industry. This is the outcome of both the better description of NO/NO_X chemistry

and improved ROHR prediction due to application of complex mechanisms.

A final comment from a general point of view is that all these 3-D CFD LES calculations are very demanding in terms of required computational power. Despite their high predictive ability with little tuning, such models are still not suitable for regular daily research/development work in a commercial sector. However, the authors expect this to change in relatively near future.

Acknowledgements

This research has been realized using the support of The Ministry of Education, Youth and Sports program NPU I (LO), project LO1311: 'Development of Vehicle Centre of Sustainable Mobility'. All the help has been gratefully appreciated.

This research has been realized using the support of Technological Agency, Czech Republic, programme National Competence Centres, project #TN01000026 Josef Bozek National Center of Competence for Surface Vehicles.

All the help has been gratefully appreciated.

List of symbols

BMEP Brake Mean Effective Pressure
CCV Cycle-to-Cycle Variation(s)
CFD Computational Fluid Dynamics
CI Compression Ignition
CNG Compressed Natural Gas
CSM Coherent Structure Model
ECFM Extended Coherent Flamlet Model
EGR Exhaust Gas Recirculation
FEM Finite Element Method
FGM Flamelet Generated Manifold
FV Finite Volume
GGPR General Gas-Phase Reactions
HR Heat Release
ICE Internal Combustion Engine
IMEP Indicated Mean Effective Pressure
ISFC Indicated Specific Fuel Consumption
LES Large Eddy Simulation
PDF Probability Density Function
PFI Port Fuel Injection
RANS Reynolds Average Navier Stokes
ROHR Rate of Heat Release
SGS Sub-grid Scale
SI Spark Ignition
TCI Turbulence-Chemistry Interaction
TPA Three-Pressure Analysis

a velocity of sound $[\mathrm{m\,s^{-1}}]$
a_T temperature conductivity $[\mathrm{m^2\,s^{-1}}]$
A area $[\mathrm{m^2}]$
c mass concentration $[\mathrm{kg\,m^{-3}}]$
c_p constant pressure thermal specific capacity
D diffusion coefficient $[\mathrm{m^2\,s^{-1}}]$
j density of diffusion flux $[\mathrm{kg\,s^{-1}\,m^{-2}}]$
q density of thermal flux $[\mathrm{W\,m^{-2}}]$
t time [s]
T temperature [K]
w velocity $[\mathrm{m\,s^{-1}}]$
x distance [m]
λ thermal conductivity $[\mathrm{W\,m^{-1}\,K^{-1}}]$
ρ density $[\mathrm{kg\,m^{-3}}]$

References

[1] M. Polášek. *Eulerovský zónový model spalovacího motoru*. Ph.D. thesis, Czech Technical University in Prague, Faculty of Mechanical Engineering, Prague, 1998. In Czech.

[2] O. Vítek. *Simulace dějů v pístovém motoru s vlivem turbulence*. Ph.D. thesis, Czech Technical University in Prague, Faculty of Mechanical Engineering, Prague, 2007. In Czech.

[3] M. Diviš. *Fuel Spray Aerodynamics in Engine Combustion Chamber*. Ph.D. thesis, Czech Technical University in Prague, Faculty of Mechanical Engineering, Prague, 2006.

[4] AVL AST. *FIRE Manual v2018*. AVL List GmbH, Graz, 2018.

[5] R. I. Issa. Solution of the implicitly discretised fluid flow equations by operator-splitting. *Journal of Computational Physics* **62**(1):40 – 65, 1986. DOI:10.1016/0021-9991(86)90099-9.

[6] O. Vítek, J. Macek, R. Tatschl, et al. Les simulation of direct injection si-engine in-cylinder flow. In *SAE Technical Papers*. 2012. DOI:10.4271/2012-01-0138.

[7] R. Tatschl, M. Bogensperger, Z. Pavlovic, et al. Les simulation of flame propagation in a direct-injection si-engine to identify the causes of cycle-to-cycle combustion variations. In *SAE Technical Papers*, vol. 2. 2013. DOI:10.4271/2013-01-1084.

[8] M. Lesieur, O. Métais, P. Comte. *Large-Eddy Simulations of Turbulence*. Cambridge University Press, Cambridge, 2005. DOI:10.1017/CBO9780511755507.

[9] H. Kobayashi. The subgrid-scale models based on coherent structures for rotating homogeneous turbulence and turbulent channel flow. *Physics of Fluids* **17**(4):045104, 2005. DOI:10.1063/1.1874212.

[10] H. Kobayashi, F. Ham, X. Wu. Application of a local SGS model based on coherent structures to complex geometries. *International Journal of Heat and Fluid Flow* **29**(3):640 – 653, 2008. DOI:10.1016/j.ijheatfluidflow.2008.02.008.

[11] J. Smagroinsky. General circulation experiments with the primitive equations, 1. The basic experiment. *Monthly Weather Review* **91**:99 – 164, 1963.

[12] J. K. Dukowicz. A particle-fluid numerical model for liquid sprays. *Journal of Computational Physics* **35**(2):229 – 253, 1980. DOI:10.1016/0021-9991(80)90087-X.

[13] S. Richard, O. Colin, O. Vermorel, et al. Towards large eddy simulation of combustion in spark ignition engines. *Proceedings of the Combustion Institute* **31**(2):3059 – 3066, 2007. DOI:10.1016/j.proci.2006.07.086.

[14] Y. Zeldovich, P. Sadovnikov, D. Frank-Kamenetskii. *Oxidation of Nitrogen in Combustion*. Publishing House of the Academy of Sciences of USSR, Moscow, 1947.

[15] F. Tap, C. Meijer, D. Goryntsev, et al. Predictive CFD modeling of diesel engine combustion using an efficient workflow based on tabulated chemistry. In *ASME Technical Paper - Internal Combustion Engine Division Fall Technical Conference*, p. V002T06A025. 2018. doi:10.1115/ICEF2018-9758.

[16] F. Tap, P. Schapotschnikow. Efficient combustion modeling based on Tabkin® CFD look-up tables: A case study of a lifted diesel spray flame. *SAE Technical Papers* 2012. doi:10.4271/2012-01-0152.

[17] O. Vitek, V. Dolecek, D. Goryntsev, et al. Application of Tabulated Detailed Chemistry to LES Model of Diesel ICE Combustion. In *ASME 2019 Internal Combustion Engine Division Fall Technical Conference*. 2019. doi:10.1115/ICEF2019-7128.

[18] J. Vavra, Z. Syrovátka, M. Takats, E. Barrientos. Scavenged pre-chamber on a gas engine for light duty truck. In *ASME 2016 Internal Combustion Engine Fall Technical Conference*. 2016. doi:10.1115/ICEF2016-9423.

[19] Z. Syrovatka, M. Takats, J. Vavra. Analysis of scavenged pre-chamber for light duty truck gas engine. *SAE Technical Papers* 2017. doi:10.4271/2017-24-0095.

[20] O. Vítek, V. Doleček, M. Diviš, J. Macek. Application of predictive combustion model to CI ICE based on LES and chemical kinetics. *MECCA : Journal of Middle European Construction and Design of Cars* **16**(2), 2018.

[21] J. Vavra, Z. Syrovatka, O. Vítek, et al. Development of a pre-chamber ignition system for light duty truck engine. *SAE Technical Papers* 2018. doi:10.4271/2018-01-1147.

[22] Z. Syrovatka, O. Vítek, J. Vavra, M. Takats. Scavenged pre-chamber volume effect on gas engine performance and emissions. *SAE Technical Papers* 2019. doi:10.4271/2019-01-0258.

[23] O. Vítek, V. Doleček, Z. Syrovátka, J. Macek. Identification of cycle-to-cycle variability sources in SI ICE based on CFD modeling. *MECCA : Journal of Middle European Construction and Design of Cars* **16**(1), 2018.

[24] J. B. Heywood. *Internal Combustion Engine Fundamentals*. McGraw-Hill, 1988.

[25] J. Vávra, I. Bortel, M. Takáts, M. Diviš. Emissions and performance of diesel–natural gas dual-fuel engine operated with stoichiometric mixture. *Fuel* **208**:722 – 733, 2017. doi:10.1016/j.fuel.2017.07.057.

[26] GT-Power User's Manual. *GT-Suite version 7.3*. Gamma Technologies Inc., 2012.

[27] O. Vitek, V. Dolecek. LES CFD modeling of diesel combustion based on detailed chemistry. In *Proceedings of KoKa*. 2019.

[28] G. P. Smith, D. M. Golden, M. Frenklach, et al. GRI-Mech. `http://www.me.berkeley.edu/gri_mech/`.